JCI insight

RESEARCH ARTICLE

Stress response protein GJA1-20k promotes mitochondrial biogenesis, metabolic quiescence, and cardioprotection against ischemia/reperfusion injury

Wassim A. Basheer,[1] Ying Fu,[1] Daisuke Shimura,[1] Shaohua Xiao,[1] Sosse Agvanian,[1] Diana M. Hernandez,[1] Tara C. Hitzeman,[1] TingTing Hong,[1,2] and Robin M. Shaw[1,2]

[1]Smidt Heart Institute, Cedars-Sinai Medical Center, Los Angeles, California, USA. [2]Department of Medicine, Cedars-Sinai Medical Center and UCLA, Los Angeles, California.

Connexin 43 (Cx43), a product of the *GJA1* gene, is a gap junction protein facilitating intercellular communication between cardiomyocytes. Cx43 protects the heart from ischemic injury by mechanisms that are not well understood. *GJA1* mRNA can undergo alternative translation, generating smaller isoforms in the heart, with GJA1-20k being the most abundant. Here, we report that ischemic and ischemia/reperfusion (I/R) injuries upregulate endogenous GJA1-20k protein in the heart, which targets to cardiac mitochondria and associates with the outer mitochondrial membrane. Exploring the functional consequence of increased GJA1-20k, we found that AAV9-mediated gene transfer of GJA1-20k in mouse hearts increases mitochondrial biogenesis while reducing mitochondrial membrane potential, respiration, and ROS production. By doing so, GJA1-20k promotes a protective mitochondrial phenotype, as seen with ischemic preconditioning (IPC), which also increases endogenous GJA1-20k in heart lysates and mitochondrial fractions. As a result, AAV9-GJA1-20k pretreatment reduces myocardial infarct size in mouse hearts subjected to in vivo ischemic injury or ex vivo I/R injury, similar to an IPC-induced cardioprotective effect. In conclusion, GJA1-20k is an endogenous stress response protein that induces mitochondrial biogenesis and metabolic hibernation, preconditioning the heart against I/R insults. Introduction of exogenous GJA1-20k is a putative therapeutic strategy for patients undergoing anticipated ischemic injury.

Introduction

Ischemic heart disease is the leading cause of mortality worldwide, with 7 million related deaths recorded in 2010, which is a 35% increase since 1990 (1). While ischemia can be intermittent and life-saving revascularization is necessary, with reperfusion the affected muscle suffers from further oxidative stress and muscle damage, a phenomenon known as ischemia/reperfusion (I/R) injury (2). There is an urgent need to protect cardiomyocytes against both ischemic and I/R injury to limit size of original myocardial infarction, preserve muscle, and prevent cardiac arrest.

Mitochondrial dysfunction is a critical component of ischemic and particularly I/R injury (3). During reperfusion, rapid reestablishment of mitochondrial membrane potential and oxidative phosphorylation causes a burst of ROS exacerbated by mitochondrial calcium overload (4) and opening of the mitochondrial permeability transition pores, leading to necrotic cell death (5, 6). Mitochondria are dynamic organelles, and it is becoming increasingly appreciated that mitochondrial function and organization of their interconnected network are crucial contributors to cell survival following metabolic stress in ischemic and I/R injury (7–12).

A prosurvival pathway in brain and heart ischemia has been associated with the C-terminus domain of the gap junction protein connexin 43 (Cx43) (13, 14), by a yet-unknown mechanism. Traditionally, Cx43 is best recognized as a cell-cell communication gap junction protein (15), which is enriched in ventricular cardiomyocytes (16) for electrical impulse transmission (17, 18). Independent of its intercellular coupling role, Cx43 has been shown to associate with the mitochondria (19–22) and to interact with mitochondrial

Conflict of interest: The authors have declared that no conflict of interest exists.

License: Copyright 2018, American Society for Clinical Investigation.

Submitted: May 1, 2018
Accepted: September 11, 2018
Published: October 18, 2018

Reference information:
JCI Insight. 2018;3(20):e121900.
https://doi.org/10.1172/jci.insight.121900.

proteins for cardiac protection (23–25). The protective role of mitochondrial Cx43 has been linked to ischemic preconditioning (IPC) (19, 20, 26–31), whereby repeated brief episodes of sublethal cycles of I/R offer cardiac muscle protection after a prolonged ischemic insult (32). The function of Cx43 in IPC has been reported not to involve intercellular communication through the gap junctions (27), yet the mechanism by which Cx43 affords metabolic protection remains poorly understood.

Cx43 is the first mammalian ion channel identified to undergo endogenous alternative translation in heart and other organs (33–35). Up to 6 smaller Cx43 isoforms are alternatively translated from the same *GJA1* mRNA in the heart (34), which initiates at downstream internal methionines, yet all end with the same Cx43 C-terminus. Given their varying sizes and biophysical properties, these C-terminal isoforms likely have functions distinct from their full-length counterpart. For instance, GJA1-20k, the most abundant small isoform of Cx43 in the heart (34), which consists of the complete C-terminal tail, is required for full-length GJA1-43k protein trafficking (34) by arranging the actin cytoskeleton to guide microtubule delivery (36). In addition, GJA1-20k has a strong tropism for mitochondria localizing to the mitochondrial membrane in close association with microtubules (37). GJA1-20k overexpression is sufficient to rescue mitochondrial localization to the cell periphery, limiting organelle network collapse upon exposure to oxidative stress (37).

Given the protective role of the Cx43 C-terminal tail in ischemic injury (13, 14), the role of Cx43 in cardiac metabolic protection (30), and the recently identified protective role of GJA1-20k on the noncardiac mitochondrial network (37), we asked whether GJA1-20k could be involved in myocardial survival when the heart is subjected to ischemic stress. In this study, we identified that GJA1-20k is an endogenous stress response protein that targets to the mitochondria in the heart and can powerfully regulate mitochondrial biogenesis and function. GJA1-20k promotes mitochondrial biogenesis while reducing mitochondrial membrane potential, respiration, and ROS production in cardiomyocytes. By doing so, GJA1-20k mimics the protective mitochondrial phenotype observed in IPC, which also results in increased endogenous GJA1-20k protein levels in heart lysates and mitochondrial fractions. Exploring the therapeutic potential of GJA1-20k, we found that pre-exposure of the heart to exogenous GJA1-20k via an AAV9 gene delivery system preconditions the myocardium, thus protecting the heart muscle from ischemic and I/R injury.

Results

GJA1-20k is an endogenous cardiac stress response protein upregulated with ischemic injury. GJA1-20k expression has been observed to increase in response to hypoxic stress in rat brains (35), but little is known about GJA1-20k in ischemic heart. We subjected ex vivo Langendorff-perfused mouse hearts to acute global I/R injury (Figure 1A, schematic), which resulted in a 56% increase in endogenous GJA1-20k protein levels (Figure 1B, quantified in Figure 1C). L-type calcium channel $Ca_v1.2$ was used as a negative control and did not change with I/R injury (Figure 1D, quantified in Figure 1E).

To evaluate GJA1-20k expression in the setting of prolonged cardiac ischemic injury, we used an in vivo mouse model with subacute ischemic cardiomyopathy induced by 3-week occlusion of the left anterior descending (LAD) coronary artery. Subacute ischemic cardiomyopathy caused a striking 5.3-fold increase in endogenous GJA1-20k protein in the heart (Figure 2, A and B). In support of this result, we also found that endogenous GJA1-20k was increased by 89% in human heart samples with chronic end-stage ischemic cardiomyopathy (Figure 2, C and D). These data indicate that GJA1-20k is an endogenous stress response protein, which upregulates with acute I/R and prolonged ischemic cardiac injury.

GJA1-20k targets mitochondria after I/R injury and associates with the outer mitochondrial membrane. We were next interested in examining where the increased endogenous GJA1-20k resides in cardiomyocytes following cardiac stress. Mouse hearts were sectioned following ex vivo I/R injury and prepared for high-resolution imaging (Figure 3A). To differentiate between endogenous GJA1-43k and GJA1-20k, we colabeled the tissue with a Cx43 N-terminus antibody, which recognizes full-length protein but not GJA1-20k (Figure 3A, Cx43-NT, red), and with a second antibody for Cx43 C-terminus, which recognizes all the isoforms (Figure 3A, Cx43-CT, green). Both antibodies can recognize full-length Cx43, which is shown as the yellow colocalization signal in the merged images of Figure 3A, whereas the smaller isoforms can be identified by green only signal. Cardiomyocytes are outlined by WGA membrane labeling (Figure 3A, indicated as dotted white lines). Interestingly, I/R results in upregulation, intracellular accumulation, and lateral redistribution of the Cx43 smaller isoforms to subsarcolemmal regions, independent of GJA1-43k (Figure 3A, green signal in the bottom right merged image). The colocalization in Figure 3A is quantified

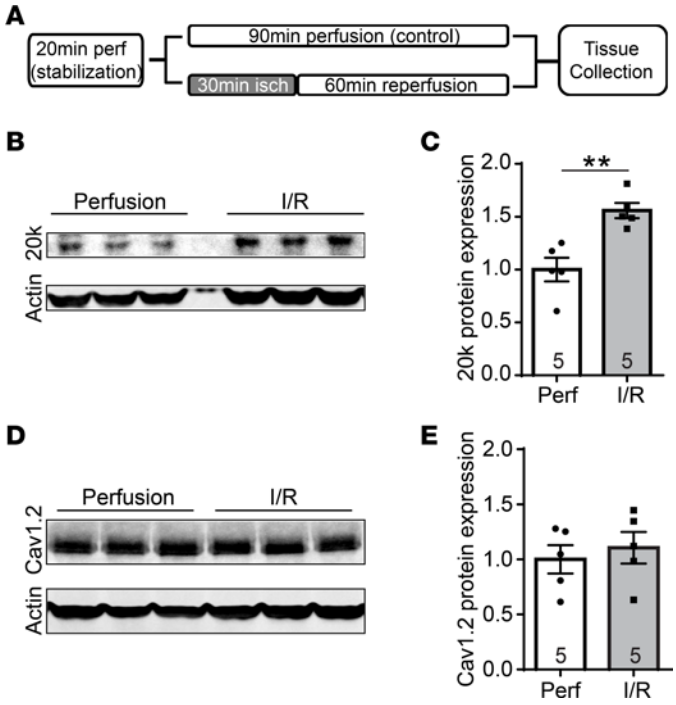

Figure 1. GJA1-20k is upregulated with acute cardiac I/R injury. (**A**) Schematic of the protocol used for I/R injury in Langendorff-perfused mouse hearts. After a 20-minute stabilization period, mouse hearts were subjected to continuous perfusion for 90 minutes as a control, or subjected to 30 minutes of ischemia followed by 60 minutes of reperfusion for I/R injury. (**B**) Western blot of heart tissue lysates after either I/R injury or control perfusion. The blots are probed with an antibody for Cx43 C-terminus and an anti-actin antibody. (**C**) Protein expression for GJA1-20k is normalized to actin and shown as fold change after I/R injury in the quantified graphs. (**D**) Western blot showing Cav1.2 protein levels in the control perfused hearts and after I/R injury. (**E**) Cav1.2 expression is normalized to actin and shown as fold change after I/R injury in the quantified graph. The number of hearts examined in **C** and **E** is shown on the graphs, and data are presented as mean fold change ± SEM. $^{**}P < 0.01$, Mann-Whitney *U* test.

by Pearson's correlation in Figure 3B, revealing a significant decrease after I/R in the Pearson's coefficient between full-length Cx43 and smaller isoforms. Together with the Western blot–identified increase in GJA1-20k (Figure 1, B and C), these data indicate that I/R-induced endogenous GJA1-20k is likely to occur in intracellular compartments distinct from full-length Cx43.

Lateralized Cx43 in the failing heart has been found in close association with mitochondria (21). The I/R-induced subcortical distribution of the small isoforms (Figure 3A), together with a reported GJA1-20k localization to mitochondria in noncardiac cells (37), prompted an exploration of whether GJA1-20k is in cardiac mitochondria. The subcellular distribution of endogenous GJA1-20k upon stress was evaluated in I/R hearts using mitochondrial biochemical fractionation (Figure 3C). Similar to the results included in Figure 1B and as evidenced in the input lysate lanes of Figure 3C (low exposure), endogenous GJA1-20k increased with I/R injury. In addition, the increase in GJA1-20k occurred in the mitochondrial fractions (Figure 3C, F2 and F3 lanes, high exposure). GJA1-20k localization to the mitochondria was further confirmed using super-resolution stochastic optical reconstruction microscopy (STORM) imaging of mitochondria isolated from adult mouse ventricular myocytes transduced with adenovirus-expressing V5-tagged GJA1-20k (Figure 3D).

To pinpoint where GJA1-20k resides once at the mitochondria, we purified mitochondria from HEK cells transfected with GFP-tagged GJA1-20k and then subjected the isolated mitochondria to a proteinase K (PK) protection assay (Figure 3E). In this assay, PK digested the proteins found in the outer mitochondrial membrane (OMM), such as Tom20, while protecting the proteins in the inner mitochondrial membrane (IMM), such as CoxIV. The isolated mitochondria expressing GFP-tagged GJA1-20k were incubated in a 1 μg/ml PK solution on ice for 30 minutes before Western blot analysis. As shown in Figure 3E, PK treatment led to reduced Tom20 levels, with no change in the amount of CoxIV. Interestingly, PK treatment completely abolished the amount of GJA1-20k at the mitochondria, as assessed using both a GFP antibody and a Cx43-CT antibody. These data indicate that GJA1-20k enrichment to mitochondria is localized to, or around, the OMM.

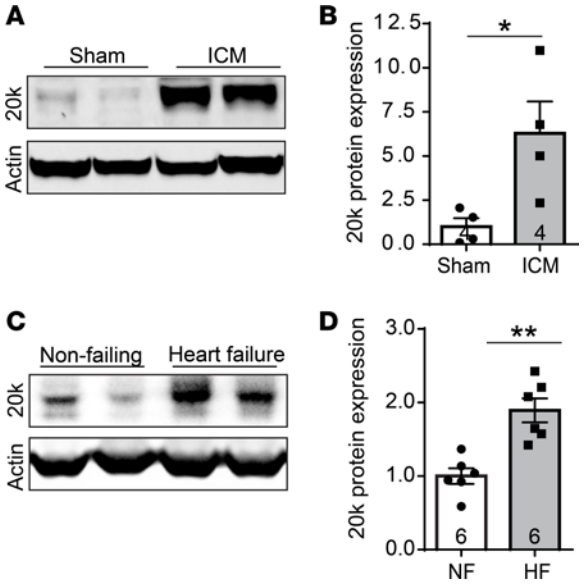

Figure 2. GJA1-20k is upregulated after subacute and chronic heart failure. (**A**) Western blot of protein lysates isolated from mouse hearts with subacute ischemic cardiomyopathy (ICM) induced by 3-week occlusion of the LAD coronary artery. The blots are probed with an antibody for Cx43 C-terminus and an actin antibody. (**B**) GJA1-20k expression is normalized to actin, and the data are shown as mean fold change ± SEM (n = 4). *P < 0.05, Mann-Whitney U test. (**C**) Western blot of protein lysates isolated from either nonfailing human hearts or hearts with end-stage ischemic cardiomyopathy. The blots are probed with a Cx43 C-terminus antibody and an actin antibody. (**D**) GJA1-20k expression is normalized to actin, and the data are shown as mean fold change ± SEM (n = 6). **P < 0.01, Mann-Whitney U test.

GJA1-20k induces mitochondrial biogenesis without altering fission protein active Drp1. Given the tropism of GJA1-20k to cardiac mitochondria, we were interested in examining the effect of exogenous GJA1-20k on mitochondrial quantity and morphology in the heart. To do so, we introduced GST-GFP control or GJA1-20k-GFP into the mouse heart in vivo by recombinant AAV9 gene transfer at 3×10^{10} vector genomes per mouse at 4 weeks prior to sacrifice (36). Expression of GFP-tagged proteins at 4 weeks after AAV9 injection was confirmed by immunofluorescence imaging of heart tissue, as shown in Figure 4A. Transmission electron microscopy imaging was then used to examine mitochondrial content in the mouse heart following GJA1-20k expression (Figure 4B). Exogenous GJA1-20k in live animals, even when expressed in the absence of metabolic stress, significantly increased the fraction of cardiomyocyte area occupied by mitochondria (Figure 4B, insets, mitochondrial area quantified in Figure 4C).

To explore whether the increased mitochondrial content is due to GJA1-20k–promoted mitochondrial biogenesis, we examined heart tissue lysates, isolated from AAV9-GST or AAV9-GJA1-20k mice, for 6 proteins associated with mitochondrial biogenesis (38, 39) (Figure 5A, quantified in Figure 5B). Of the 6, 5 were significantly increased in the GJA1-20k group, including a 66% increase in peroxisome proliferator–activated receptor-γ coactivator-1 α (PGC-1α) and a 39% increase in the mitochondrial encoded cytochrome C oxidase II (mtCO2) (P < 0.01). PGC-1α is known to be the intranuclear generated mitochondrial biogenesis "master regulator" (38). Only the increase in nuclear respirator factor 1 (NRF1) was not significant. NRF1 is downstream of PGC-1α; however, their expression profiles do not always correlate (39). De novo mitochondrial biogenesis is further supported by the evidence that AAV9-GJA1-20k also resulted in a significant 25% increase in mitochondrial DNA copy number in heart tissue, as assessed using real-time PCR (Figure 5C). These data indicate that GJA1-20k can activate the transcriptional pathways to promote mitochondrial biogenesis in the heart.

Having such a robust effect on mitochondrial biogenesis raises the important question of whether GJA1-20k regulates mitochondrial dynamics in relation to mitochondrial fusion and fission, which can further contribute to new mitochondrial biogenesis (40). We therefore examined the expression level of the fission protein active form of Drp1 (41) and fusion protein Mitofusin1 (42) in the F3 mitochondrial fraction isolated from AAV9-GST and AAV9-GJA1-20k hearts (Figure 6A). As indicated in Figure 6, AAV9-GJA1-20k did not alter the amount of active Drp1 or the amount of Mitofusin1. However, exogenous expression of AAV9-GJA1-20k did result in a significant 2.8-fold increase in Tom20 levels in the mitochondrial fraction, as compared with the GST control, which is consistent with the observed upregulation of Tom20 in whole heart lysate as well (Figure 5). These results indicate that GJA1-20k–induced mitochondrial biogenesis does not involve Drp1-dependent mitochondrial fission.

GJA1-20k lowers mitochondrial membrane potential, respiration, and ROS production. Next, to further assess the effect of GJA1-20k on mitochondrial function and cardiac metabolism, we evaluated mitochondrial membrane potential in cardiomyocytes isolated from hearts expressing AAV9-GST or

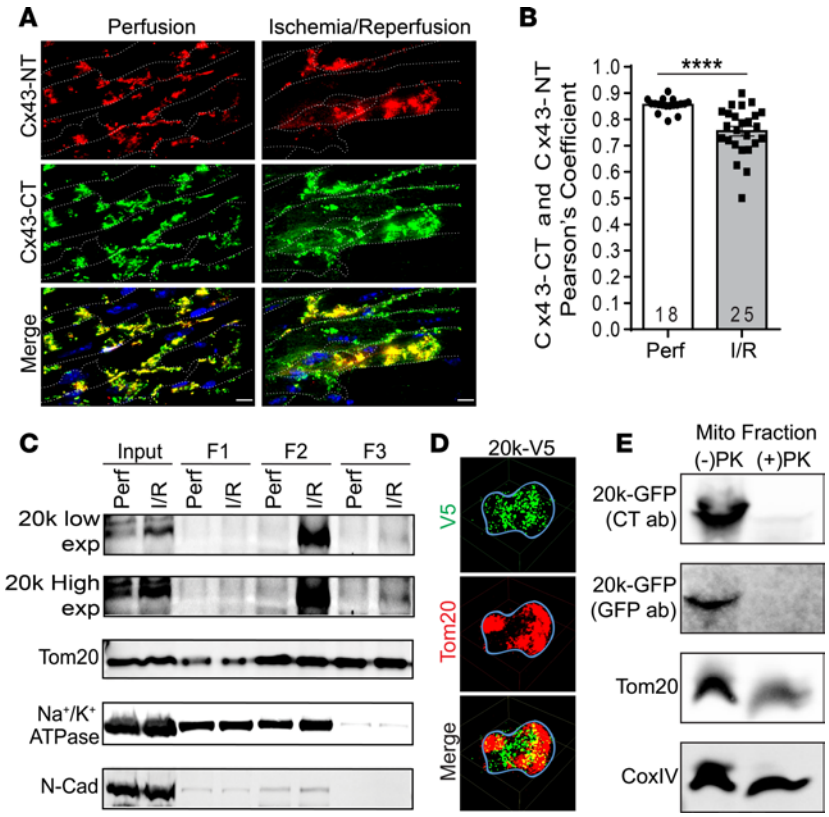

Figure 3. GJA1-20k targets mitochondria after I/R injury and associates with the OMM. (**A**) Confocal images of mouse heart cryosections following I/R injury. Tissue is costained with a Cx43 N-terminus antibody (Cx43-NT, red) and a Cx43 C-terminus antibody (Cx43-CT, green), and cell membranes are labeled with WGA (white dotted line). Scale bar: 10 μm. Pearson's coefficient for the colocalization signal (yellow, merged images) is quantified in **B**. Data are mean ± SEM (number of cells quantified is shown on the graph). ****$P < 0.0001$, unpaired *t* test. (**C**) Biochemical fractionation of isolated hearts after I/R, showing GJA1-20k protein distribution in the supernatant prior to ultracentrifugation (F1) versus mitochondrial fractions (F2, F3). Low- and high-exposure blots of GJA1-20k are shown as well as mitochondrial marker (Tom20) and plasma membrane markers (Na^+/K^+ATPase and N-cadherin). (**D**) 3D STORM images of a single cardiac mitochondrion (outlined with a blue line) expressing V5-tagged GJA1-20k (green). Tom20 is shown in red. Scale bar: 0.5 μm. (**E**) Western blot of mitochondrial fractions isolated from HEK cells transfected with GFP-tagged GJA1-20k and subjected to a proteinase K protection assay (1 μg/ml PK on ice for 30 minutes). PK treatment completely abolished GJA1-20k at the outer mitochondrial membrane (OMM), as assessed using GFP and Cx43-CT antibodies. Tom20 is used as an OMM marker and CoxIV is used as an inner mitochondrial membrane marker.

AAV9-GJA1-20k (Figure 7, A and B). JC-1 is a MitoTracker dye that selectively enters mitochondria and reversibly changes color from red (active mitochondria) to green (nonactive mitochondria) as membrane potential decreases. Thus, the red/green fluorescence ratio of JC-1 identifies the fraction of active mitochondria at a given time point. As observed in Figure 7A, ratiometric measurement (red to green) confirmed a lower mitochondrial membrane potential in GJA1-20k–expressing cardiomyocytes (Figure 7B), indicating a lower metabolic state.

Cardiomyocyte metabolism was also evaluated using the Seahorse XF Cell Mito Stress assay, which measures oxygen consumption rate. As seen in Figure 7, C and D, the Seahorse data indicate that GJA1-20k significantly reduces mitochondrial maximal respiratory capacity, inducing a lower metabolic state.

Finally, mitochondrial metabolic function was also assessed in the cardiomyocytes isolated from hearts expressing AAV9-GST or AAV9-GJA1-20k by examining basal levels of mitochondria-generated ROS, using confocal microscopy and MitoSOX dye as a fluorescent indicator. MitoSOX Red is a fluorogenic dye that specifically targets to mitochondria in live cells and is only oxidized in the presence of superoxide agents to produce red fluorescence. Therefore, the more superoxide agents present in the cell, the higher the fluorescence intensity produced by MitoSOX. The data in Figure 7, E and F, indicate that exogenous expression of GJA1-20k reduced ROS production by the mitochondria, further supporting the results in Figure 7, A–D, that GJA1-20k induced

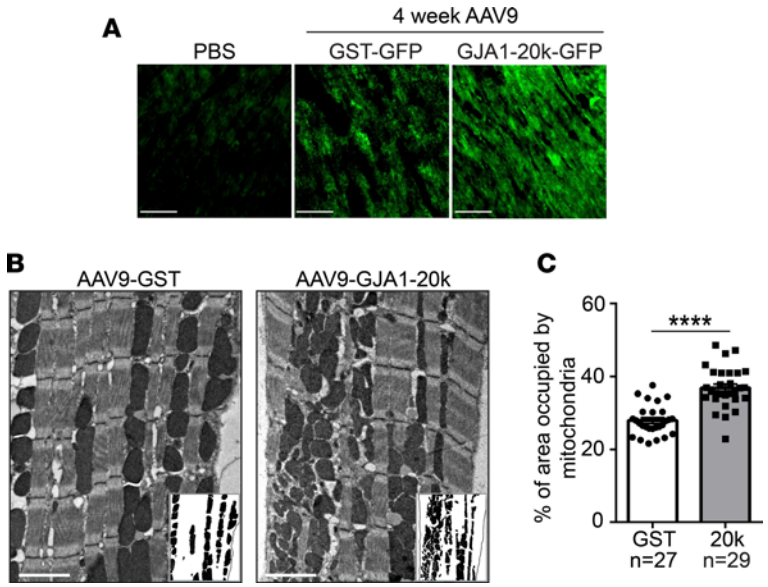

Figure 4. GJA1-20k increases mitochondrial content. (**A**) GST-GFP control or GJA1-20k-GFP are introduced into the heart by the recombinant AAV9 gene delivery system at 3×10^{10} vector genomes per mouse. Immunofluorescence confocal imaging of heart tissue confirms the expression of the GFP-tagged proteins at 4 weeks after AAV9 expression as compared with a PBS control heart with no AAV9. Scale bar: 50 μm. (**B**) Electron microscope images of left ventricular tissue isolated from AAV9-GJA1-20k– or AAV9-GST–expressing mouse hearts. Insets show mitochondria, with cardiomyocyte area outlined using a black line. Scale bar: 2 μm. (**C**) Quantification of the percentage area of the cardiomyocyte occupied by mitochondria in each group (number of images assessed is shown on the graph). Data in **C** are mean ± SEM. $^{**}P < 0.01$, $^{****}P < 0.0001$, unpaired *t* test.

mitochondrial hibernation. Taken together, our results in Figure 7 suggest that GJA1-20k induces metabolic quiescence, which may reduce workload on each mitochondrion and, therefore, results in decreased ROS production. By doing so, GJA1-20k can offer cardioprotective effects in the setting of ischemic and I/R injury.

GJA1-20k protects heart from ischemic injury in vivo. Given the apparent protective effect of GJA1-20k on inducing mitochondrial biogenesis and metabolic quiescence, we evaluated GJA1-20k's potential for muscle preservation by assessing infarct size in an in vivo myocardial ischemic model induced by LAD coronary artery occlusion. Seventy-two hours after LAD ligation, AAV9-GJA1-20k– or AAV9-GST–expressing mice were sacrificed, and infarct size was determined by triphenyl tetrazolium chloride (TTC) staining of transverse ventricular slices. TTC stains healthy viable heart muscle deep red, while areas of infarctions are pale. Infarct size was quantified as a percentage of total slice area, corrected by slice weight (Figure 8). Relative to animals injected with control AAV9-GST, infarct size was significantly reduced in animals that received AAV9-GJA1-20k (20.4% ± 2.8% vs. 34.9% ± 1.8% in the GST control group) ($P < 0.01$). This result indicates that prior introduction of exogenous GJA1-20k can precondition the heart and protect it against ischemic injury.

On the other hand, lower mitochondrial membrane potential and respiration at baseline (Figure 7, A–D) also raised the concern of whether extended GJA1-20k expression may ultimately lead to cardiac pathology. To address this issue, we performed echocardiography imaging on AAV9-GJA1-20k– or AAV9-GST–expressing hearts at 4 weeks following AAV9 introduction; the results are summarized in Supplemental Figure 1 (supplemental material available online with this article; https://doi.org/10.1172/jci.insight.121900DS1). We found that at baseline treatment with GJA1-20k did not result in any changes in the measured functional and structural cardiac parameters as compared with the AAV9-GST control hearts. These data indicate that, even though the expression of GJA1-20k at baseline drives the mitochondria into a stress-resistant state, it does not lead to cardiac dysfunction or the development of a myopathy. It is possible that the GJA1-20k–mediated increase in mitochondrial content (Figures 4–6) can compensate for less metabolic active individual mitochondria (Figure 7) to maintain normal net cellular energy output in normal hearts.

GJA1-20k increases with IPC, contributing to IPC-mediated cardiac protection in an ex vivo model of I/R injury. Our findings that GJA1-20k promoted mitochondrial biogenesis (Figures 4–6) and metabolic quiescence (Figure 7), with a reduction in infract size (Figure 8), are analogous to the reported protective mitochondrial

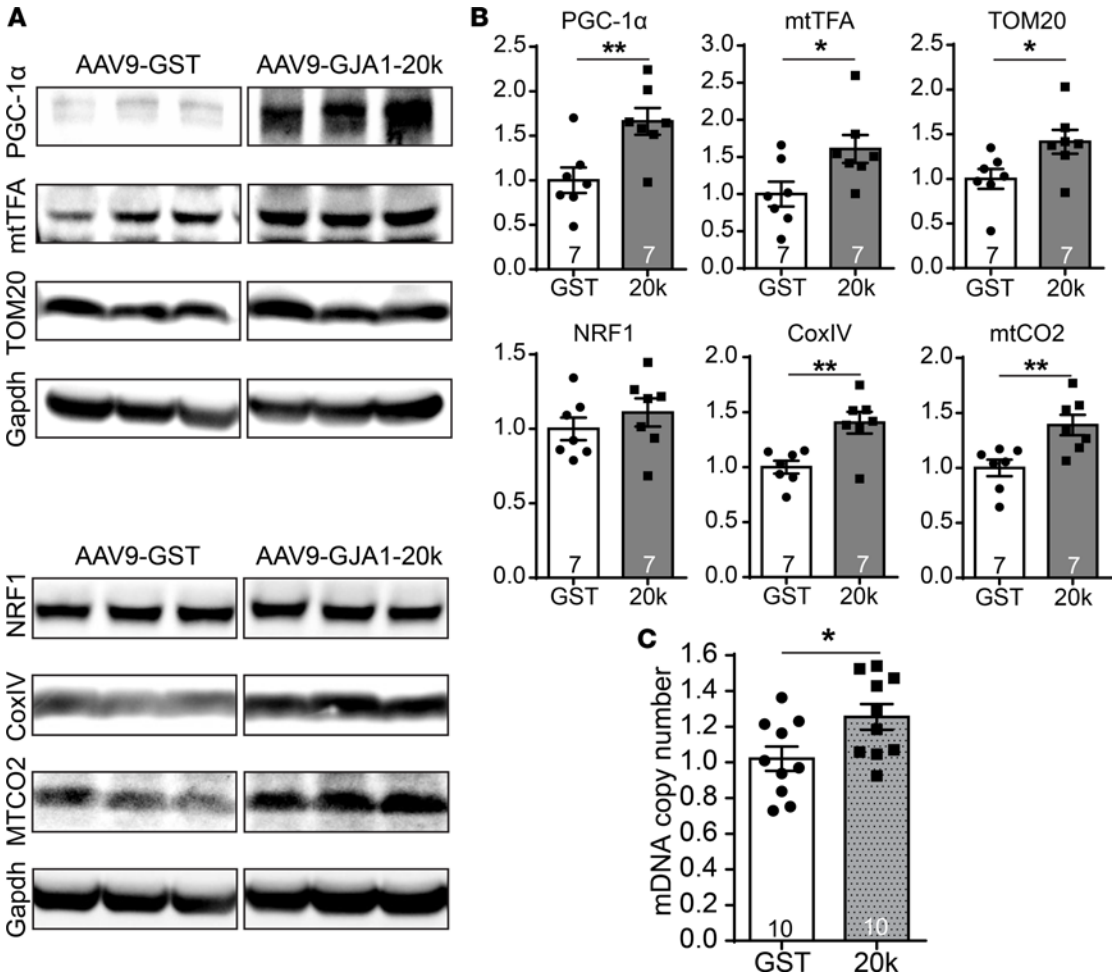

Figure 5. GJA1-20k promotes mitochondrial biogenesis. (**A**) Western blots showing the expression level of critical transcription factors involved in mitochondrial biogenesis (PGC1-1α, mtTFA, and NRF1) and mitochondrial proteins (TOM20, CoxIV, and mtCO2) in heart lysates from AAV9-GJA1-20k or AAV9-GST mice. Quantification of protein expression is shown in **B** as fold change after normalization to Gapdh (n = 7 hearts for each treatment). (**C**) Real-Time PCR data showing mitochondrial DNA copy number in heart tissue isolated from AAV9-GJA1-20k and AAV9-GST mice (n = 10). Data in **B** and **C** are mean ± SEM. *P < 0.05, **P < 0.01, unpaired t test.

phenotype triggered by IPC (43–46). This prompted us to examine if GJA1-20k is part of the IPC pathway. We induced IPC in ex vivo Langendorff-perfused mouse hearts and examined endogenous GJA1-20k levels by Western blot in total heart lysates as well as in mitochondrial fractions isolated from these hearts. As shown in Figure 9A and quantified in Figure 9B, IPC resulted in a 2.5-fold increase in endogenous GJA1-20k protein levels in total heart lysates, as compared with the control perfused hearts. Consistent with that observed in the total heart lysates, IPC also resulted in a 2-fold increase in GJA1-20k protein level in the F3 mitochondrial fraction, as shown in Figure 9C and quantified in Figure 9D. These data suggest that GJA1-20k is involved in the IPC pathway mediating cardioprotection.

Establishing that GJA1-20k is part of the IPC signaling pathway (Figure 9) led us to investigate whether in vivo expression of GJA1-20k in the heart is sufficient to protect the myocardium from I/R injury to a similar extent as that seen with an IPC stimulus. We therefore evaluated size of infarction in Langendorff-perfused hearts isolated from AAV9-GST– or AAV9-GJA1-20k–administered mice, with the hearts subjected to ex vivo I/R injury alone or I/R with IPC. Infarct size was determined by TTC staining of transverse ventricular slices and quantified as a percentage of total slice area, corrected by slice weight (Figure 10, A and B). Exogenous AAV9-GJA1-20k expression in the heart resulted in a 47% decrease in infarct size as compared with the AAV9-GST–expressing hearts after I/R injury (P < 0.001), consistent with the in vivo infarct size data in Figure 8. Subjecting the AAV9-GST hearts to IPC prior to the prolonged I/R insult resulted in a 37% decrease in infarct size as compared with the control AAV9-GST hearts without IPC (P < 0.05).

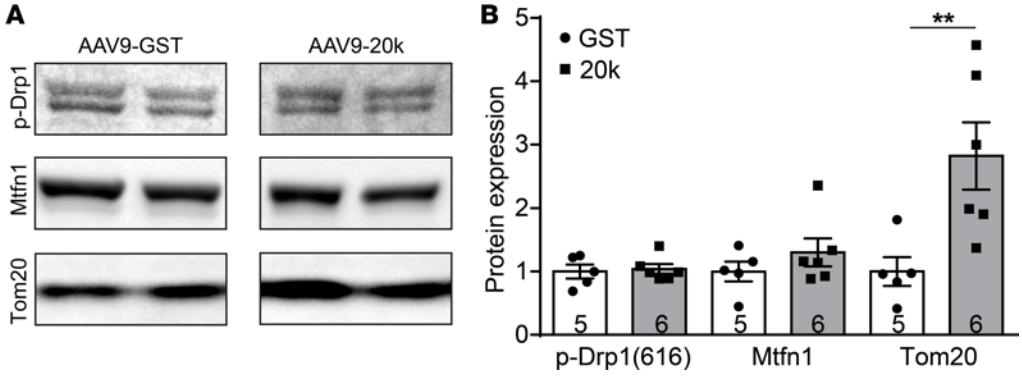

Figure 6. GJA1-20k does not affect the amount of active Drp1 fission protein or Mitofusin1 fusion protein. (**A**) Western blot showing amount of active Drp1 fission protein, Mitofusin1 fusion protein, and Tom20 in the F3 mitochondrial fraction isolated from AAV9-GST or AAV9-GJA1-20k hearts. Quantification of protein band intensity is shown in **B** as fold change (n = 5 for GST and n = 6 for 20k hearts). Data in **B** are mean ± SEM. $^{**}P < 0.01$, Kruskal-Wallis test.

Left ventricular end diastolic pressure (LVEDP) and left ventricular developed pressure (LVDP) were also recorded in hearts from the 3 different treatment groups (AAV9-GST+IR, AAV9-GST+IPC+IR, and AAV9-20k+IR). As indicated in Figure 10, C and D, in the AAV9-GST+IR group, I/R resulted in a substantial elevation in LVEDP (Figure 10C) concurrent with a drop in LVDP (Figure 10D), with a partial recovery of LVEDP toward the end of the 60-minute reperfusion period, indicating a severe hypocontractile state in the control hearts during I/R. Pretreatment of the heart with AAV9-GJA1-20k significantly prevented the elevation in LVEDP during the first 30 minutes of the reperfusion phase, while strongly preserving the elevation of LVDP throughout the reperfusion phase, as compared with the AAV9-GST+IR group. On the other hand, subjecting the AAV9-GST–expressing hearts to IPC also prevented I/R-induced elevation in LVEDP and reduction in LVDP (Figure 10C). Taken together, the data in Figure 10 indicate that pre-exposure of the heart to GJA1-20k is sufficient to reproduce the IPC effect in preserving cardiac muscle and protecting diastolic and systolic heart function from I/R injury.

Discussion

In this study, we identified GJA1-20k as an endogenous stress response protein in the heart (Figures 1 and 2) that targets to the mitochondria and associates with the OMM (Figure 3), promotes mitochondrial biogenesis (Figures 4–6), induces metabolic quiescence (Figure 7), and reduces ROS generation (Figure 7). By doing so, GJA1-20k preconditioned the myocardium and strongly protected the heart muscle from ischemic and I/R injury, as observed in both in vivo (Figure 8) and ex vivo (Figure 10) mouse models. Mitochondrial regulation by GJA1-20k, a protein that was only recently recognized to exist by alternative translation (33–35), provides mechanistic insight into how the otherwise traditional Cx43 gap junction protein can play diverse noncanonical roles, such as ensuring cell survival.

The role of GJA1-20k in cardiac metabolism and muscle protection during stress. It has been reported that siRNA-mediated knockdown of Cx43 mRNA in adipocytes, which knocks down the smaller isoforms as well (34), reduces mitochondrial content while increasing oxidative stress (47). Our results in Figures 4–7 are consistent with this earlier finding and suggest that increased GJA1-20k enhances mitochondrial biogenesis and reduces ROS production, which is important for survival of the stressed myocardium (48). A greater number of mitochondria may allow for a better functional reserve and reduce the burden of oxidative damage each mitochondrion faces in the setting of ischemic and I/R insults. In addition, by producing less damaging levels of mitochondria-generated ROS (49), GJA1-20k can protect the heart by limiting opening of the mitochondrial permeability transition pores and protecting against cell death as a result of ischemic and oxidative stress (5).

The data in Figures 4–6 suggest that GJA1-20k can increase de novo mitochondrial biogenesis without affecting mitochondrial fusion and fission, particularly Drp1-mediated fission. Accumulating evidence indicates that Drp1-dependent mitochondrial fission is a prerequisite for mitophagy (50, 51), and it has been reported that efficient mitophagy may act as a prerequisite for mitochondrial biogenesis, which, in turn, is cardioprotective for I/R injury (52). Without affecting active Drp1 (Figure 4), GJA1-

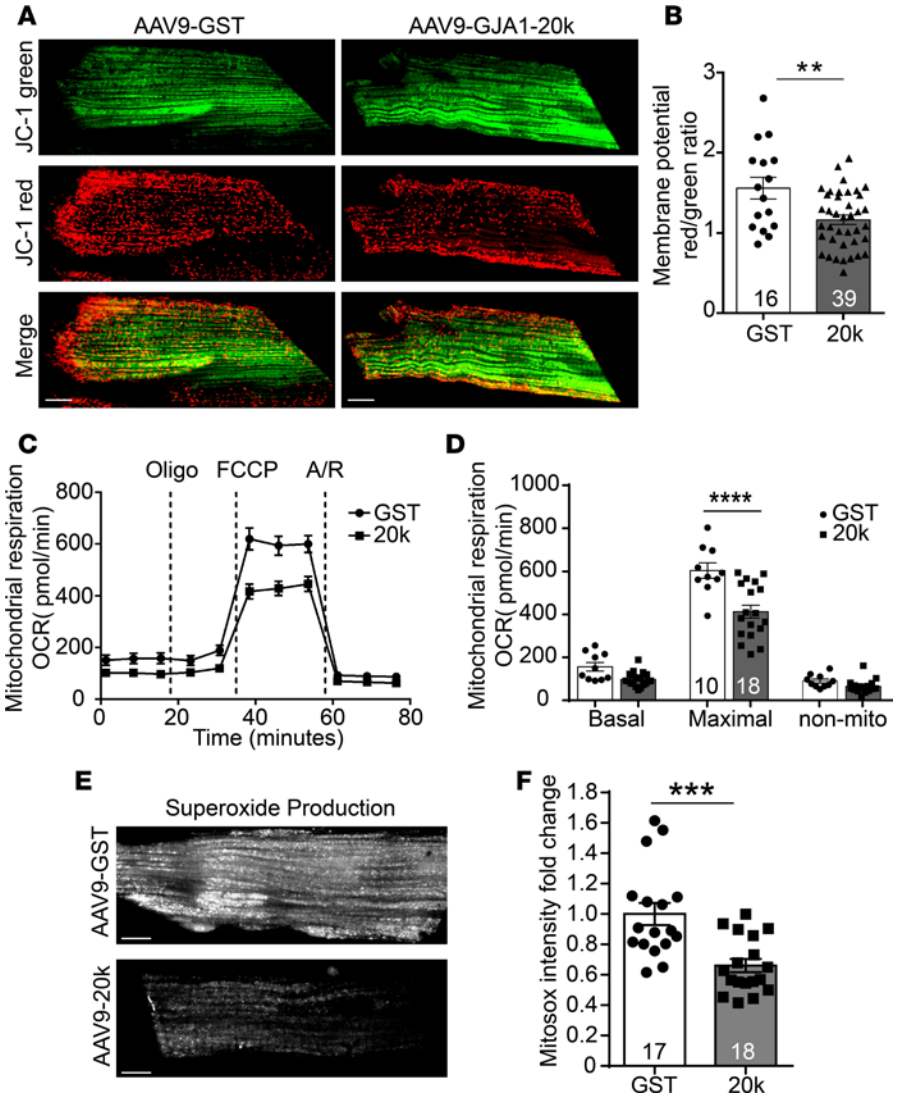

Figure 7. GJA1-20k promotes mitochondrial quiescence. (**A**) Cardiomyocytes isolated from AAV9-GJA1-20k– or AAV9-GST–expressing hearts were loaded with JC-1 MitoTracker dye, which selectively enters mitochondria and reversibly changes color from JC-1 red to JC-1 green as the membrane potential decreases. (**B**) Ratiometric measurement (red/green) using JC-1 in the two groups (number of cells quantified is shown on the graph). Data are mean ± SEM. $^{**}P < 0.01$, unpaired *t* test. (**C**) Seahorse XF Cell Mito Stress assay is used for characterization of oxygen consumption rate (OCR) in cardiomyocytes isolated from AAV9-GJA1-20k or AAV9-GST hearts. OCR under basal conditions and in response to the indicated mitochondrial inhibitors is shown overtime. (**D**) Quantification of basal respiration, maximal respiratory, and nonmitochondrial respiration between the two groups. Data are mean ± SEM (number of wells assessed per group is shown on the graph). $^{****}P < 0.0001$, 2-way ANOVA. (**E**) Cardiomyocytes isolated from AAV9-GJA1-20k– or AAV9-GST–expressing hearts were loaded with the fluorogenic dye MitoSOX Red to examine mitochondrial superoxide production by assessing fluorescence intensity, which is quantified in **F** as fold change ($n = 17$ cells for GST and $n = 18$ cells for 20k hearts). Data in **F** are mean ± SEM. $^{***}P < 0.001$, unpaired *t* test. Scale bar: 10 μm.

20k is less likely to be involved in this Drp1-dependent fission and mitophagy pathway for mitochondrial biogenesis and cardioprotection. On the other hand, although Drp1 is the main contributor of mitochondrial division in the cells (41, 53–55), there is emerging evidence that some of the mitochondrial fission and associated mitophagy can occur in the absence of Drp1 (54, 56). For instance, in addition to inducing constriction of the mitochondrial membrane, leading to subsequent Drp1-mediated fission (55), it is possible for the actin cytoskeleton to create contractile rings resulting in mitochondrial fission

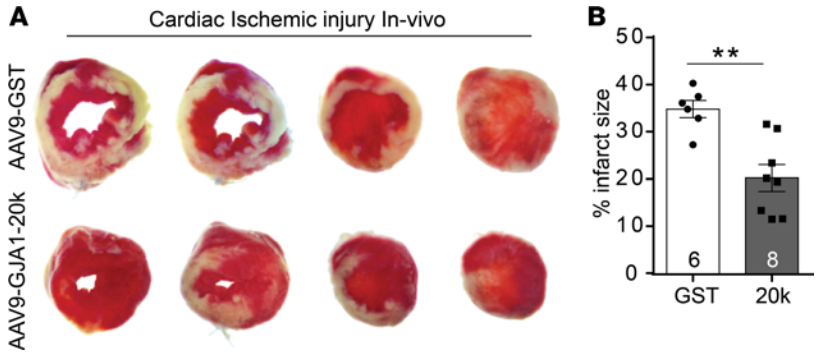

Figure 8. GJA1-20k protects the heart from ischemic injury in vivo. (**A**) Representative images of transverse slices of TTC-stained hearts from AAV9-GJA1-20k– and AAV9-GST–expressing mice at 72 hours after in vivo myocardial infarction induced by LAD coronary artery occlusion. TTC stains viable heart muscle deep red while areas of infarction are pale. (**B**) Infarct size is quantified as a percentage of total slice area, corrected by slice weight (GST, $n = 6$ hearts; 20k, $n = 8$ hearts). Data are shown as mean ± SEM. $^{**}P < 0.01$, Mann-Whitney *U* test.

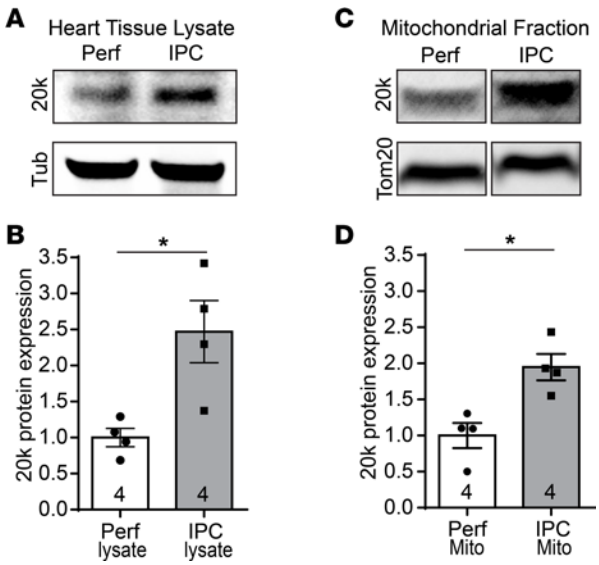

Figure 9. GJA1-20k increases with ischemic preconditioning. Western blots of total tissue lysates (**A**) or F3 mitochondrial fractions (**C**) isolated from Langendorff-perfused mouse hearts, which were subjected to either ischemic preconditioning (IPC) or continuous perfusion (Perf) as a control. The blots are probed with a Cx43 C-terminus antibody to detect endogenous GJA1-20k, with a tubulin antibody, or with a Tom20 antibody. (**B**) Protein expression for GJA1-20k in **A** is normalized to tubulin and shown as fold change. $n = 4$ hearts per group. Data are shown as mean ± SEM. $^*P < 0.05$, Mann-Whitney *U* test. (**D**) Protein expression for GJA1-20k in **C** is normalized to Tom20 and shown as fold change. $n = 4$ hearts per group. Data are shown as mean ± SEM. $^*P < 0.05$, Mann-Whitney *U* test.

by sheer force generation, independent of Drp1 activity (54). Thus, via regulating the actin cytoskeleton (36) and associating with the OMM (Figure 3E), GJA1-20k may still affect mitochondrial fission by helping tether actin to the OMM. It would be interesting in future studies to decipher such mechanisms underlying the interplay among GJA1-20k, the actin cytoskeleton, and mitochondrial division.

While the existence of GJA1-20k can help explain the role of Cx43 in protection of cardiac metabolism (30), future studies are needed to understand the tropism of GJA1-20k to mitochondria and how it induces biogenesis and reduces respiration simultaneously. In other studies, it has been identified that GJA1-20k is necessary for the trafficking of full-length Cx43 to the intercalated disc (34, 36) as well as to de novo gap junctions in epithelial cells (57) and endometrial cells (58). The mechanism of GJA1-20k trafficking appears to involve regulation of cytoskeleton organization (36). GJA1-20k may be a potent scaffolding protein, organizing the interaction among cytoskeleton, membrane, and vesicles containing Cx43 channel (34) or organelles such as mitochondria (37). Future investigation of cytoskeleton regulation of mitochondrial activity, with GJA1-20k mediation, should be particularly interesting.

GJA1-20k is a potential translatable therapy alternative to IPC. A classic cardioprotective response to nonlethal ischemic insult, such that occurs with preconditioning stimulus, is to induce myocardial hibernation (44, 59). The metabolic state of hibernation is marked by mitochondrial quiescence (44). In addition, pharmacological inhibition of electron transport chain complexes, which reduces mitochondrial metabolic activity, has been reported to improve tissue survival and functional recovery after ischemia (60). During IPC, the mitochondria can be primed into a hibernating stress-resistant state, leading to reduced cell death following I/R injury (44, 45). The preconditioned mitochondrial phenotype is characterized by depolarization of the inner membrane of the mitochondria, which subsequently leads to decreased membrane potential and reduced mitochondrial activity (44). The reduction in mitochondrial respiration within the preconditioned myocardium (46) causes decreased ROS generation (44), limiting opening of the mitochondrial permeability transition pores and protecting against cell death (5, 6). In addition to mitochondrial quiescence, IPC has been reported to promote mitochondrial biogenesis in the heart as a mechanism of ischemic protection (43). The effects of GJA1-20k on mitochondrial biogenesis, metabolic function, and cardioprotection are very similar to the reported phenotype triggered by IPC (43–46). Indeed, we found that endogenous GJA1-20k was increased with IPC in total heart lysates (Figure 9, A and B) as well as in mitochondrial fractions (Figure 9, C and D) isolated from ex vivo Langendorff-perfused mouse hearts, suggesting that GJA1-20k is an important component of the protective pathway triggered by IPC.

A striking finding of the current study is that exogenous GJA1-20k, induced by gene transfer, can mimic the cardiac protective effect of IPC (Figures 8 and 10) by inducing metabolic quiescence and limiting production of damaging levels of mitochondrial ROS (49) (Figure 7). The ability for GJA1-20k–expressing cells to enter an adaptive hibernating state may effectively reduce energy substrate utilization and oxygen

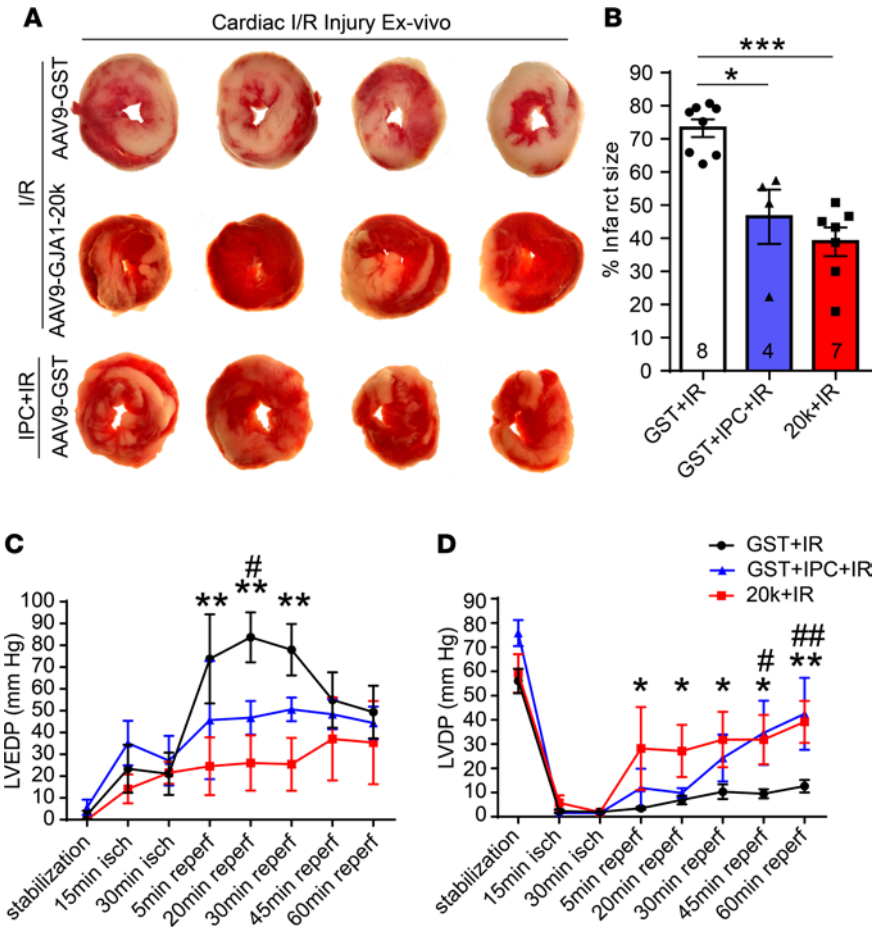

Figure 10. GJA1-20k mimics the IPC protective phenotype seen in heart ex vivo I/R injury. (**A**) Representative transverse slices of TTC-stained cardiac sections from Langendorff-perfused hearts isolated from AAV9-GST– or AAV9-GJA1-20k–expressing mice and subjected to ex vivo I/R injury alone (30-minute ischemia and 60-minute reperfusion) or to IPC stimulus prior to the prolonged I/R injury. (**B**) Infarct size is quantified as a percentage of total slice area, corrected by slice weight (number of hearts quantified per group in shown on the graph). Data are shown as mean ± SEM. $^{*}P < 0.05$, $^{***}P < 0.001$, Kruskal-Wallis test. (**C**) Left ventricular end diastolic pressure (LVEDP) and (**D**) left ventricular developed pressure (LVDP) measurements during I/R in Langendorff-perfused hearts isolated from AAV9-GST– or AAV9-GJA1-20k–expressing mice. The hearts were subjected to ex vivo I/R injury alone or to 4 cycles of IPC followed by I/R. GST+IR compared with 20k+IR is indicated by either * or **, and GST+IR compared with GST+IPC+IR is indicated by either # or ##. $^{*}P < 0.05$, $^{\#}P < 0.05$, $^{**}P < 0.01$, $^{\#\#}P < 0.01$, 2-way ANOVA. Data are mean ± SEM (GST+I/R, $n = 6$ hearts; GST+IPC+IR, $n = 4$ hearts; 20k+IR, $n = 5$ hearts).

demand to match the ATP-depleted and hypoxic environment. At the same time, with increased mitochondrial content due to GJA1-20k–induced mitochondrial biogenesis, the overall cellular energy output can be maintained for normal cellular function, preserving systolic and diastolic function of AAV9-GJA1-20k–transduced hearts at both baseline (Supplemental Figure 1) and after I/R injury (Figure 10, C and D). These data suggest use of GJA1-20k as a therapeutic approach to increase cardiomyocyte survival during anticipated ischemic stress without compromising cardiac function.

Although IPC can protect mitochondrial content from I/R injury (61), a protection that lasts for hours (62), direct use of IPC in a patient's heart can be detrimental. Use of GJA1-20k is an attractive therapeutic alternative to IPC. Future studies will be necessary to identify fast and efficient delivery approaches, such as direct myocardial application of GJA1-20k protein. For instance, previous studies have demonstrated that a peptide mimetic of the carboxyl-terminus of Cx43 can be applied directly to the injured heart using an adherent methylcellulose patch to reduce gap junction remodeling and arrhythmia after ventricular injury (63). It is possible that a similar GJA1-20k protein gel patch can be developed and directly applied to the myocardium during heart surgery and anticipated reperfusion procedures.

Methods

A detailed Methods section is available in the Supplemental Methods.

Isolation of adult mouse ventricular cardiomyocytes. Adult (12- to 14-week-old) male C57BL/6 mice (The Jackson Laboratory, 000664) were injected with heparin (100 IU, i.p.) 20–30 minutes before dissection. Mice were anesthetized with isoflurane, cervical dislocation was performed, and hearts were removed rapidly and immersed in ice-cold calcium-free perfusion buffer. Hearts were retrogradely perfused through the aorta and digested with collagenase II (2 mg/ml) according to a previously established method (64). The ventricular tissue was then gently dispersed into cell suspension and centrifuged at 40 *g* for 3 minutes. Damaged myocytes and nonmyocytes were removed by a series of washes in buffer containing, sequentially, 100, 400, or 900 μmol/l $CaCl_2$. Cardiomyocytes were pelleted by centrifugation at 40 *g* for 3 minutes after each wash. After the final wash, cardiomyocytes were resuspended in cardiomyocyte culture medium, plated onto dishes precoated with 10 μg/ml laminin, and maintained for 2 hours in 37°C incubator with 5% CO_2 to allow them to adhere.

Immunostaining and confocal imaging. For tissue immunofluorescence, cryosections (10 μm) were fixed in 4% PFA for 20 minutes at room temperature, blocked and permeabilized at room temperature for 1 hour, and incubated with primary antibodies at 4°C overnight. The primary antibodies used were mouse anti-Cx43 (N-terminus epitope, 1:200, Acris AM32558SU-N), rabbit anti-Cx43 (C-terminus epitope, 1:1,000, MilliporeSigma, C6219), and chicken anti-GFP (1:500, Abcam, ab13970). The following day, the sections were incubated for 1 hour at room temperature with the respective secondary antibodies conjugated to anti-mouse or anti-rabbit Alexa Fluor (1:500, Life Technologies) and coverslips were mounted using ProLong gold antifade reagent containing DAPI (Thermo Fisher Scientific). The tissue sections were imaged using a Nikon Eclipse T*i* imaging system with a ×100/1.49 Apo objective. Maximum intensity projections of 12.5 μm confocal *Z*-stacks were obtained for imaging. Colocalization signal between Cx43-CT and Cx43-NT signal was assessed using JACoP (Just Another Colocalization Plugin) for ImageJ.

Mitochondria purification from heart. Mitochondria was isolated according to a previously established method (65). In brief, mouse hearts or isolated cardiomyocytes were manually homogenized in isolation buffer A with BSA ([in mM] 230 mannitol, 70 sucrose, 10 HEPES, 2 EDTA, pH 7.2, with KOH and 1 mg/ml fatty acid–free BSA) using a Potter Elvehjem homogenizer. The homogenate was centrifuged at 1,300 *g* for 3 minutes at 4°C, and 10% of the supernatant was removed as input and stored at –80°C. The remaining supernatant was centrifuged at 10,000 *g* for 10 minutes at 4°C. The resulting pellet, which contained crude mitochondria, was gently resuspended in 55 μl isolation buffer A with no BSA, while the supernatant which contains the F1 cytosol fraction was stored at –80°C. The resuspended crude mitochondria pellet was gently overlaid on 3 ml of 30% (vol/vol) Percoll solution in buffer B (250 mM sucrose, 10 mM HEPES, 1 mM EDTA-Na2, pH 7.4) (0.9 ml Percoll [MilliporeSigma] pure + 2.1 ml buffer B). The mitochondria were ultracentrifuged at 50,000 *g* for 45 minutes at 4°C. After the ultracentrifugation, 2 clear layers of mitochondria were observed, F2 and F3. The F2 and F3 fractions were carefully collected in separate tubes and resuspended in isolation buffer A (without BSA) and centrifuged at 12,000 *g* for 5 minutes at 4°C. The resulting pellet from each fraction was washed twice with 1 ml of isolation buffer A (without BSA) to remove all Percoll and then resuspended in RIPA lysis buffer and stored with Nupage LDS sample buffer at –80°C.

PK protection assay. HEK293T cells (Life Technologies) were transfected with GFP-tagged GJA1-20k, and mitochondria were isolated using the mitochondria isolation kit for cultured cells with Dounce homogenization method (Thermo Fisher Scientific, 89874) (66). The isolated mitochondria expressing GFP-tagged GJA1-20k were incubated in a 1 μg/ml PK solution (diluted in buffer C provided with the mitochondria isolation kit) on ice for 30 minutes before they were processed for biochemical protein analysis.

Super resolution STORM imaging. The crude mitochondria pellet isolated from adult mouse ventricular cardiomyocytes, infected with an adenovirus vector for V5-GJA1-20k, was resuspended in isolation buffer A and plated onto a laminin-precoated 35-mm glass-bottom dish for 1:30 hours at 4°C. The mitochondria were then fixed with 4% PFA at room temperature for 10 minutes, followed by blocking and permeabilization for 10 minutes at room temperature in 1% NGS with 0.5% TritonX-100 in PBS. The mitochondria were then incubated at 4°C overnight with primary antibodies diluted in 1% NGS with 0.1% TritonX-100 in PBS. Primary antibodies used were rabbit anti-Tom20 (1:200; Santa Cruz biotechnologies, sc11415) and mouse anti-V5 (1:200, MilliporeSigma, V8012). The following day, the mitochondria were incubated for 1 hour at room temperature with the respective secondary antibodies conjugated to anti-mouse or anti-rabbit Alexa Fluor (1:500, Life Technologies), and after 6 washes (5 minutes each) in PBS, the mitochondria were left to air dry and then stored in the dark at room temperature. At the day of STORM imaging, freshly made oxygen-scavenging buffer system was added

to the mitochondria-containing dishes to enable effective photoswitching. Briefly, 10 mmol/l cysteamine (MilliporeSigma) was added to GLOX (0.5 mg/ml glucose oxidase, 40 μg/ml catalase, 10% glucose) in 50 mmol/l Tris (pH 8.0) buffer with 10 mmol/l NaCl. All images were collected using a Nikon Eclipse Ti microscope with a ×100 objective with 1.49 numerical aperture total internal reflection fluorescent objective (67). The STORM module in Nikon Element software was used to obtain and analyze the images to generate 3D projections of V5-20K/Tom20 and V5-GFP/Tom20 images at high resolution (*XY* resolution, 10–20 nm; *Z* resolution, 50 nm).

Western blotting. Heart tissues were lysed in either RIPA buffer (50 mM Tris, 150 mM NaCl, 1 mM EDTA, 1% TritonX-100, 1% sodium deoxycholate, 1 mM NaF, 0.2 mM Na_3VO_4, and Halt Protease and Phosphatase Inhibitor Cocktail (Thermo Fisher Scientific) or mitochondrial isolation buffer A with BSA. The samples were incubated at room temperature for 45 minutes and then subjected to SDS-PAGE electrophoresis using NuPAGE Bis-Tris gels (4%–12%) with MOPS or MES running buffers (Invitrogen) according to the manufacturer's instructions. Gels were transferred to FluoroTrans PVDF membranes (Pall) and blocked for 1 hour at room temperature with 5% nonfat milk or 5% BSA (for phospho antibodies) in TNT buffer (0.1% Tween20, 150 mM NaCl, 50 mM Tris, pH 8.0). Membranes were then incubated overnight with primary antibodies diluted in 5% milk or 5% BSA in TNT. Primary antibodies used were rabbit anti-actin (1:3,000, MilliporeSigma, A2103), rabbit anti-$CaV_{1.2}$ (1:500, Alomone Labs, ACC-003), mouse anti-Cx43 (1:1,000, Fred Hutchinson Cancer Research Center, CT1), mouse anti–N-cadherin (1:1,000, BD Biosciences, 610921), mouse anti-Na^+/K^+ ATPase (1:1,000, MilliporeSigma, 05-369), rabbit anti-Tom20 (1:1,000, Santa Cruz Biotechnologies, sc1145), rabbit anti-PGC-1α (1:1,000, Novus Biologicals, NBP1-04676), rabbit anti-NRF1 (1:5000, Abcam, ab175932), rabbit anti-mtCO2 (1:500, Abcam, ab198286), rabbit anti-mtTFA (1:1,000, Abcam, ab138351), mouse anti-CoxIV (1:1,000, Abcam, ab14744), mouse anti-Gapdh (1:5000, Abcam, ab8245), rabbit-anti p-Drp1(Ser616; active form of Drp1) (1:500, Cell Signaling, D9A1), chicken anti-Mitofusin1 (1:500, Abcam, ab107129), mouse anti-tubulin (1:1,000, MilliporeSigma, T6199). The following day, the membranes were incubated for 1 hour at room temperature with the respective secondary antibodies (anti-rabbit or anti-mouse Alexa Fluor 1:500, Life Technologies) diluted in 5% milk or 5% BSA in TNT. Membranes were imaged using the Versadoc MP 4000 fluorescent Western detection system (Bio-Rad). Quantity One (Bio-Rad) analysis software was used to quantify individual band intensities. The samples were normalized to actin or Gapdh, graphs were plotted as fold change, and statistical analysis was performed using GraphPad Prism 6 software.

AAV9 production and gene delivery. AAV9 vectors containing GST-GFP or GJA1-20k-GFP driven by the CMV promoter were produced in HEK 293 cells and were purified by Welgen Inc. Adult C57BL/6 male mice received 100 μl of 3×10^{10} vector genomes of AAV9-GST-GFP or AAV9-GJA1-20k-GFP through retro-orbital injection (36). The AAV9 vectors were delivered 4 weeks prior to cardiomyocyte or heart tissue collection and analysis. Vector-encoded GFP expression in heart tissue was confirmed by immunofluorescence detection at 4 weeks after injection.

Transmission electron microscopy. Left ventricular tissue was isolated from AAV9-GST-GFP or AAV9-GJA1-20k-GFP mice with AAV9 vectors delivered 4 weeks prior to tissue collection. Hearts were perfused with 2% glutaraldehyde and 2% paraformaldehyde in PBS for 10 minutes, and left ventricular tissue was post-fixed with 1% osmium tetroxide and incubated in 3% uranyl acetate (37). Samples were then dehydrated in ethanol, treated with propylene oxide, embedded in Spurr resin (Electron Microscopy Services), and sectioned using an ultramicrotome (Leica). Sections were mounted on EM grids and stained with uranyl acetate and lead citrate and prepped for imaging.

Images were acquired using the JEM1200-EX JEOL microscope equipped with a digital camera (BioScan 600W, Gatan). Percentage of cell area occupied by mitochondria was assessed using ImageJ (NIH). All electron microscopy work was done by the core facility at the Electron Imaging Center of The California NanoSystems Institute, UCLA.

Assessment of mitochondrial DNA copy number. Genomic DNA was extracted from heart tissue isolated from AAV9-GJA1-20k– and AAV9-GST–expressing mice using the NucleoSpin Tissue kit (MACHEREY-NAGEL, 740952). Mitochondrial copy number was then assessed using the Mouse Mitochondrial DNA Copy Number Assay Kit according to the manufacture's instructions (Detroit R&D, MCN3) and a Real-Time PCR system (Bio-Rad, CFX-Connect) (38).

Measurement of mitochondrial membrane potential. Acutely isolated cardiomyocytes from AAV9-GST– or AAV9-GJA1-20k–expressing hearts were loaded with MitoTracker JC1 (Thermo Fisher Scientific) at 5 μg/ml (in perfusion buffer with 1.8 mM $CaCl_2$) and incubated at 37°C in a humidified atmosphere of

5% CO_2 for 30 minutes (68). Cells were washed 3 times (with perfusion buffer containing 1.8 mM $CaCl_2$) before live-cell imaging. The cardiomyocytes were imaged using a Nikon Eclipse T*i* imaging system with a ×100/1.49 Apo objective. Maximum intensity projections of 12.5 μm confocal *Z*-stacks were obtained for imaging. The ratio of red to green fluorescence intensity was used as indicator of mitochondrial membrane potential and quantified using ImageJ (NIH).

Seahorse mitochondrial respiration assay. The mitochondrial oxygen consumption was evaluated using Seahorse XF Cell Mito stress test kit according to the manufactures' instructions (69). Briefly, 24-well Agilent Seahorse cell culture microplates were coated with 20 μg/μl laminin overnight. Adult cardiomyocytes (1,000 cells) isolated from AAV9-GST or AAV9-GJA1-20k hearts were plated in each well and allowed attachment for 1 hour. The cells were then switched to XF base media supplemented with 5.5 mM glucose, 1 mM pyruvate, and 4 mM L-glutamine and incubated in 0% CO_2 for 1 hour before the test. FCCP (carbonyl cyanide p-trifluoromethoxyphenylhydrazone) at 0.8 μM was used to elicit maximal respiration. Complex I and III inhibitors (rotenone and antimycin A) were used at 50 μM to measure nonmitochondrial respiration. ATPase synthase inhibitor oligomycin at 3 μM does not inhibit oxygen consumption, consistent with the state-4 like bioenergetic profile of quiescent adult cardiomyocytes (69).

Superoxide measurement. Acutely isolated cardiomyocytes from AAV9-GST– or AAV9-GJA1-20k–expressing hearts were loaded with MitoSOX Red (Thermo Fisher Scientific) at 5 μg/ml (in perfusion buffer with 1.8 mM $CaCl_2$) and incubated at 37°C in a humidified atmosphere of 5% CO_2 for 20 minutes. Cells were washed 3 times (with perfusion buffer containing 1.8 mM $CaCl_2$) before live-cell imaging. The cardiomyocytes were imaged using a Nikon Eclipse T*i* imaging system with a ×100/1.49 Apo objective. Maximum intensity projections of 12.5 μm confocal *Z*-stacks were obtained for imaging. The red fluorescence intensity was used as indicator of mitochondrial superoxide production and quantified using ImageJ (NIH).

Echocardiography. Transthoracic echocardiography imaging was performed on anesthetized animals using a VEVO 3100 ultrasound machine with MX5550D transducer (VisualSonics) (70). Left ventricular volume, %EF, %FS, and heart rate measurements were determined from the B-mode long axis view. LVID, LVPW, LVAW, and left ventricular mass measurements were determined from the M-mode short axis view.

Langendorff-perfused mouse heart preparation, IPC, and I/R injury. Adult (12- to 14-week-old) male C57BL/6 mice (The Jackson Laboratory, 000664) were injected with heparin (100 IU, i.p.) 20–30 minutes prior to the Langendorff procedure (71, 72). Mice were anesthetized with isoflurane, cervical dislocation was performed, and hearts were removed quickly by a midsternal incision and placed into ice-cold modified pH 7.4 Krebs-Henseleit (K-H) solution. The heart was attached to a Langendorff apparatus (Radnoti) and perfused through the aorta at a constant rate of 2.5 ml/min with the K-H buffer. The K-H solution was constantly gassed with 95% O_2/5% CO_2. Perfusion medium was passed through water-jacketed tubing and cylinders, and the temperature was maintained at 37°C with a temperature-controlled circulating water bath. The hearts were allowed to equilibrate for 20 minutes to achieve a steady state before they were subjected to 30 minutes of global ischemia, followed by 60 minutes of reperfusion. Control hearts were perfused continuously throughout the protocol. During no-flow ischemia, the heart was immersed in warm K-H buffer in order to maintain warmth and moisture.

For the IPC experiments, the isolated mouse hearts were allowed to equilibrate for 20 minutes to achieve a steady state before they were subjected to 4 repeated cycles of 3.5-minute ischemia followed by 5-minute reperfusion (31). After preconditioning, the hearts were subjected to prolonged I/R of 30-minute ischemia and 60-minute reperfusion.

For ECG recordings, electrodes (140155-M, Radnoti) were used to record the electrocardiogram and heart rate throughout the experiment using labchart software (ADInstruments) with Power lab and Bio Amp hardware (ADInstruments). A Millar MIKRO-TIP (SPR-671) pressure catheter (Millar Instruments) was inserted into the left ventricle from the left atrium to measure left ventricular pressure throughout the experiment using a Bridge Amp (ADInstruments). LVEDP, LVDP, and heart rate were monitored and recorded continuously using PowerLab system (ADInstruments). Hearts were paced at 360 beats per minute using a pacing electrode (140157M, Radnoti) and a stimulus delivered from a stimulator (stimulus isolator, ADInstruments). After the initial 20-minute stabilization, hearts were excluded from further study if they exhibited one or more of the following exclusion criteria: LVEDP higher than 20 mmHg; LVDP less than 50 mmHg; intrinsic heart rate less than 280 bpm; or irregular heart rate; or aortic regurgitation. Hearts were then subjected to 30 minutes of global ischemia followed by 1 hour of reperfusion. Pacing was initiated at 2 minutes after reperfusion.

Myocardial infarction model. Four weeks after AAV9-GST-GFP or AAV9-GJA1-20k-GFP delivery, mice were given a dose of analgesia (0.1 mg/kg Buprenex and 5 mg/kg Carprofen), injected with an anesthetic cocktail (10 mg/kg xylazine and 100 mg/kg ketamine), intubated using the Biolite intubation system (Braintree Scientific), and mechanically ventilated at 0.2 cm^3 tidal volume/100 respirations per minute with oxygen and isoflurane inhaled anesthesia (Minivent type 845, Harvard Apparatus). LAD coronary artery ligation was performed as previously described (73). Complete occlusion of the vessel was verified by visible blanching of the myocardium distal to the tie. After verifying that the mice were breathing spontaneously, they were injected with analgesia (Buprenex) and observed until recovery was complete. No animals died due to surgery. At 72 hours after ligation, mice were euthanized, and hearts were collected for infarct size analysis.

Infarct size analysis. TTC staining was used for postmortem determination of infarct size. Transverse heart slices 1-millimeter thick were immersed in freshly made 1% TTC solution for 20 minutes at 37°C, followed by fixation (10% neutral formalin, MilliporeSigma) for 30 minutes before imaging. Using ImageJ (NIH), the area of the infarcted region of each slice was manually traced, measured, and expressed as a percentage of the total slice area. Infarct size was corrected to the weight of each slice as follows: weight infarct = (WeightSlice 1 × %InfarctSlice 1) + (WeightSlice 2 × %InfarctSlice 2) + (WeightSlice 3 × %InfarctSlice 3) + (WeightSlice 4 × %InfarctSlice 4) (74).

Human tissue collection. Cold cardioplegia was perfused antegrade prior to cardiectomy, and the explanted heart was placed immediately in ice-cold physiologic solution. Full-thickness samples from the left ventricle were obtained, placed in cryovials, and immediately submerged in liquid nitrogen to snap freeze before storage at –80°C.

Statistics. All quantitative data were expressed as mean ± SEM and analyzed using Prism 6 software (GraphPad). For comparison between two groups, unpaired 2-tailed Student's *t* test or Mann-Whitney *U* test was performed. For comparison between three groups, Kruskal-Wallis test with Dunn's multiple comparisons test was performed. The Seahorse data in Figure 7, C and D, and the intraventricular pressure data in Figure 10, C and D, were analyzed using 2-way ANOVA with Sidak's or Holm-Sidak's multiple comparisons test. Shapiro-Wilk normality test was performed for all data. Two-sided *P* values are reported, and a *P* value of less than 0.05 was deemed statistically significant.

Study approval. C57BL/6 mice were maintained under sterile barrier conditions. All procedures were reviewed and approved by Cedars-Sinai Medical Center Institutional Animal Care and Use Committee. Deidentified human heart lysates from patients with end-stage ischemic cardiomyopathy undergoing transplantation and nonfailing controls who died from noncardiac reasons were obtained from the Cedars-Sinai Heart Institute Biobank, which stores plasma as well as tissue and lysates from heart explants acquired under informed consent using a protocol approved by institutional review board from the Cedars-Sinai Medical Center Office of Research Compliance.

Author contributions

All authors contributed to writing the manuscript. WAB and YF contributed to the manuscript by designing research studies, conducting experiments, acquiring data, and analyzing data. DS and SX contributed to the manuscript by conducting experiments and analyzing data. SA and DMH contributed to the manuscript by conducting experiments. TCH contributed to the statistical analysis of the data. TTH and RMS contributed to the manuscript by designing research studies and analyzing data.

Acknowledgments

We thank S. Ryazantsev at the Electron Imaging Center at California NanoSystems Institute of UCLA for his expertise in electron microscopy; the CURE Vector Core Facility at UCLA (CURE/P30 DK041301) for production of adenoviruses; D. Taylor and A. Andres from the Cedars-Sinai Metabolism and Mitochondrial Research Core; and B. Sun for technical assistance with coronary artery ligation in the ischemia mouse model. This work was supported by NIH grants HL094414 and HL138577 (to RMS) and HL133286 (to TTH) and by American Heart Association grants 13EIA4480016 (to RMS), 16BGIA27770151 and 16IRG27780031 (to TTH), and 12SDG12080084 (to YF).

Address correspondence to: Robin Shaw, 8700 Beverly Boulevard, 1016 Plaza Level, Davis Building, Los Angeles, California 90048, USA. Phone: 310.967.3842; Email: robin.shaw@cshs.org.

1. Wong ND. Epidemiological studies of CHD and the evolution of preventive cardiology. *Nat Rev Cardiol*. 2014;11(5):276–289.
2. Bolli R, Patel BS, Jeroudi MO, Lai EK, McCay PB. Demonstration of free radical generation in "stunned" myocardium of intact dogs with the use of the spin trap alpha-phenyl N-tert-butyl nitrone. *J Clin Invest*. 1988;82(2):476–485.
3. Walters AM, Porter GA, Brookes PS. Mitochondria as a drug target in ischemic heart disease and cardiomyopathy. *Circ Res*. 2012;111(9):1222–1236.
4. Griffiths EJ, et al. Mitochondrial calcium transporting pathways during hypoxia and reoxygenation in single rat cardiomyocytes. *Cardiovasc Res*. 1998;39(2):423–433.
5. Halestrap AP, Clarke SJ, Javadov SA. Mitochondrial permeability transition pore opening during myocardial reperfusion--a target for cardioprotection. *Cardiovasc Res*. 2004;61(3):372–385.
6. Joiner ML, et al. CaMKII determines mitochondrial stress responses in heart. *Nature*. 2012;491(7423):269–273.
7. Wai T, et al. Imbalanced OPA1 processing and mitochondrial fragmentation cause heart failure in mice. *Science*. 2015;350(6265):aad0116.
8. Gomes LC, Di Benedetto G, Scorrano L. During autophagy mitochondria elongate, are spared from degradation and sustain cell viability. *Nat Cell Biol*. 2011;13(5):589–598.
9. Jezek P, Plecitá-Hlavatá L. Mitochondrial reticulum network dynamics in relation to oxidative stress, redox regulation, and hypoxia. *Int J Biochem Cell Biol*. 2009;41(10):1790–1804.
10. Ong SB, Hall AR, Hausenloy DJ. Mitochondrial dynamics in cardiovascular health and disease. *Antioxid Redox Signal*. 2013;19(4):400–414.
11. Rambold AS, Kostelecky B, Lippincott-Schwartz J. Together we are stronger: fusion protects mitochondria from autophagosomal degradation. *Autophagy*. 2011;7(12):1568–1569.
12. Ong SB, Subrayan S, Lim SY, Yellon DM, Davidson SM, Hausenloy DJ. Inhibiting mitochondrial fission protects the heart against ischemia/reperfusion injury. *Circulation*. 2010;121(18):2012–2022.
13. Kozoriz MG, et al. The connexin43 C-terminal region mediates neuroprotection during stroke. *J Neuropathol Exp Neurol*. 2010;69(2):196–206.
14. Maass K, Chase SE, Lin X, Delmar M. Cx43 CT domain influences infarct size and susceptibility to ventricular tachyarrhythmias in acute myocardial infarction. *Cardiovasc Res*. 2009;84(3):361–367.
15. Rohr S. Role of gap junctions in the propagation of the cardiac action potential. *Cardiovasc Res*. 2004;62(2):309–322.
16. Beyer EC, Paul DL, Goodenough DA. Connexin43: a protein from rat heart homologous to a gap junction protein from liver. *J Cell Biol*. 1987;105(6 Pt 1):2621–2629.
17. Gutstein DE, et al. Heterogeneous expression of Gap junction channels in the heart leads to conduction defects and ventricular dysfunction. *Circulation*. 2001;104(10):1194–1199.
18. Shaw RM, Rudy Y. Ionic mechanisms of propagation in cardiac tissue. Roles of the sodium and L-type calcium currents during reduced excitability and decreased gap junction coupling. *Circ Res*. 1997;81(5):727–741.
19. Boengler K, et al. Connexin 43 in cardiomyocyte mitochondria and its increase by ischemic preconditioning. *Cardiovasc Res*. 2005;67(2):234–244.
20. Rodriguez-Sinovas A, et al. Translocation of connexin 43 to the inner mitochondrial membrane of cardiomyocytes through the heat shock protein 90-dependent TOM pathway and its importance for cardioprotection. *Circ Res*. 2006;99(1):93–101.
21. Hesketh GG, et al. Ultrastructure and regulation of lateralized connexin43 in the failing heart. *Circ Res*. 2010;106(6):1153–1163.
22. Soetkamp D, et al. S-nitrosation of mitochondrial connexin 43 regulates mitochondrial function. *Basic Res Cardiol*. 2014;109(5):433.
23. Boengler K, et al. Mitochondrial connexin 43 impacts on respiratory complex I activity and mitochondrial oxygen consumption. *J Cell Mol Med*. 2012;16(8):1649–1655.
24. Denuc A, et al. New protein-protein interactions of mitochondrial connexin 43 in mouse heart. *J Cell Mol Med*. 2016;20(5):794–803.
25. Martins-Marques T, Anjo SI, Pereira P, Manadas B, Girão H. Interacting network of the gap junction (GJ) Protein connexin43 (Cx43) is modulated by ischemia and reperfusion in the heart. *Mol Cell Proteomics*. 2015;14(11):3040–3055.
26. Schwanke U, Konietzka I, Duschin A, Li X, Schulz R, Heusch G. No ischemic preconditioning in heterozygous connexin43-deficient mice. *Am J Physiol Heart Circ Physiol*. 2002;283(4):H1740–H1742.
27. Li X, Heinzel FR, Boengler K, Schulz R, Heusch G. Role of connexin 43 in ischemic preconditioning does not involve intercellular communication through gap junctions. *J Mol Cell Cardiol*. 2004;36(1):161–163.
28. Dhein S. New, emerging roles for cardiac connexins. Mitochondrial Cx43 raises new questions. *Cardiovasc Res*. 2005;67(2):179–181.
29. Heinzel FR, et al. Impairment of diazoxide-induced formation of reactive oxygen species and loss of cardioprotection in connexin 43 deficient mice. *Circ Res*. 2005;97(6):583–586.
30. Rodríguez-Sinovas A, Ruiz-Meana M, Denuc A, García-Dorado D. Mitochondrial Cx43, an important component of cardiac preconditioning. *Biochim Biophys Acta*. 2018;1860(1):174–181.
31. Rodríguez-Sinovas A, et al. Effects of substitution of Cx43 by Cx32 on myocardial energy metabolism, tolerance to ischaemia and preconditioning protection. *J Physiol (Lond)*. 2010;588(Pt 7):1139–1151.
32. Murry CE, Jennings RB, Reimer KA. Preconditioning with ischemia: a delay of lethal cell injury in ischemic myocardium. *Circulation*. 1986;74(5):1124–1136.
33. Salat-Canela C, Sesé M, Peula C, Ramón y Cajal S, Aasen T. Internal translation of the connexin 43 transcript. *Cell Commun Signal*. 2014;12:31.
34. Smyth JW, Shaw RM. Autoregulation of connexin43 gap junction formation by internally translated isoforms. *Cell Rep*. 2013;5(3):611–618.
35. Ul-Hussain M, et al. Internal ribosomal entry site (IRES) activity generates endogenous carboxyl-terminal domains of Cx43 and is responsive to hypoxic conditions. *J Biol Chem*. 2014;289(30):20979–20990.
36. Basheer WA, et al. GJA1-20k arranges actin to guide Cx43 delivery to cardiac intercalated discs. *Circ Res*. 2017;121(9):1069–1080.
37. Fu Y, et al. Cx43 Isoform GJA1-20k promotes microtubule dependent mitochondrial transport. *Front Physiol*. 2017;8:905.
38. Medeiros DM. Assessing mitochondria biogenesis. *Methods*. 2008;46(4):288–294.
39. Stetler RA, et al. Mitochondrial biogenesis contributes to ischemic neuroprotection afforded by LPS pre-conditioning. *J Neurochem*.

2012;123 Suppl 2:125–137.
40. Ventura-Clapier R, Garnier A, Veksler V. Transcriptional control of mitochondrial biogenesis: the central role of PGC-1alpha. *Cardiovasc Res*. 2008;79(2):208–217.
41. Zaja I, et al. Cdk1, PKCδ and calcineurin-mediated Drp1 pathway contributes to mitochondrial fission-induced cardiomyocyte death. *Biochem Biophys Res Commun*. 2014;453(4):710–721.
42. Papanicolaou KN, et al. Cardiomyocyte deletion of mitofusin-1 leads to mitochondrial fragmentation and improves tolerance to ROS-induced mitochondrial dysfunction and cell death. *Am J Physiol Heart Circ Physiol*. 2012;302(1):H167–H179.
43. McLeod CJ, Pagel I, Sack MN. The mitochondrial biogenesis regulatory program in cardiac adaptation to ischemia--a putative target for therapeutic intervention. *Trends Cardiovasc Med*. 2005;15(3):118–123.
44. Kelly RF, Sluiter W, McFalls EO. Hibernating myocardium: is the program to survive a pathway to failure? *Circ Res*. 2008;102(1):3–5.
45. Halestrap AP, Clarke SJ, Khaliulin I. The role of mitochondria in protection of the heart by preconditioning. *Biochim Biophys Acta*. 2007;1767(8):1007–1031.
46. da Silva MM, Sartori A, Belisle E, Kowaltowski AJ. Ischemic preconditioning inhibits mitochondrial respiration, increases H2O2 release, and enhances K+ transport. *Am J Physiol Heart Circ Physiol*. 2003;285(1):H154–H162.
47. Kim SN, et al. Connexin 43 is required for the maintenance of mitochondrial integrity in brown adipose tissue. *Sci Rep*. 2017;7(1):7159.
48. Bayeva M, Gheorghiade M, Ardehali H. Mitochondria as a therapeutic target in heart failure. *J Am Coll Cardiol*. 2013;61(6):599–610.
49. Brookes PS, Yoon Y, Robotham JL, Anders MW, Sheu SS. Calcium, ATP, and ROS: a mitochondrial love-hate triangle. *Am J Physiol, Cell Physiol*. 2004;287(4):C817–C833.
50. Pi H, et al. Dynamin 1-like-dependent mitochondrial fission initiates overactive mitophagy in the hepatotoxicity of cadmium. *Autophagy*. 2013;9(11):1780–1800.
51. Frank M, et al. Mitophagy is triggered by mild oxidative stress in a mitochondrial fission dependent manner. *Biochim Biophys Acta*. 2012;1823(12):2297–2310.
52. Zhou H, Zhu P, Wang J, Zhu H, Ren J, Chen Y. Pathogenesis of cardiac ischemia reperfusion injury is associated with CK2α-disturbed mitochondrial homeostasis via suppression of FUNDC1-related mitophagy. *Cell Death Differ*. 2018;25(6):1080–1093.
53. Smirnova E, Griparic L, Shurland DL, van der Bliek AM. Dynamin-related protein Drp1 is required for mitochondrial division in mammalian cells. *Mol Biol Cell*. 2001;12(8):2245–2256.
54. Roy M, Itoh K, Iijima M, Sesaki H. Parkin suppresses Drp1-independent mitochondrial division. *Biochem Biophys Res Commun*. 2016;475(3):283–288.
55. Hatch AL, Gurel PS, Higgs HN. Novel roles for actin in mitochondrial fission. *J Cell Sci*. 2014;127(Pt 21):4549–4560.
56. Yamashita SI, et al. Mitochondrial division occurs concurrently with autophagosome formation but independently of Drp1 during mitophagy. *J Cell Biol*. 2016;215(5):649–665.
57. James CC, Zeitz MJ, Calhoun PJ, Lamouille S, Smyth JW. Altered translation initiation of Gja1 limits gap junction formation during epithelial-mesenchymal transition. *Mol Biol Cell*. 2018;29(7): 797–808.
58. Nadeem L, Shynlova O, Mesiano S, Lye S. Progesterone via its type-A receptor promotes myometrial gap junction coupling. *Sci Rep*. 2017;7(1):13357.
59. Depre C, Vatner SF. Cardioprotection in stunned and hibernating myocardium. *Heart Fail Rev*. 2007;12(3-4):307–317.
60. Chen Q, Hoppel CL, Lesnefsky EJ. Blockade of electron transport before cardiac ischemia with the reversible inhibitor amobarbital protects rat heart mitochondria. *J Pharmacol Exp Ther*. 2006;316(1):200–207.
61. Boengler K, et al. Prevention of the ischemia-induced decrease in mitochondrial Tom20 content by ischemic preconditioning. *J Mol Cell Cardiol*. 2006;41(3):426–430.
62. Pagliaro P, Gattullo D, Rastaldo R, Losano G. Ischemic preconditioning: from the first to the second window of protection. *Life Sci*. 2001;69(1):1–15.
63. O'Quinn MP, Palatinus JA, Harris BS, Hewett KW, Gourdie RG. A peptide mimetic of the connexin43 carboxyl terminus reduces gap junction remodeling and induced arrhythmia following ventricular injury. *Circ Res*. 2011;108(6):704–715.
64. Smyth JW, et al. Actin cytoskeleton rest stops regulate anterograde traffic of connexin 43 vesicles to the plasma membrane. *Circ Res*. 2012;110(7):978–989.
65. Singh H, et al. Visualization and quantification of cardiac mitochondrial protein clusters with STED microscopy. *Mitochondrion*. 2012;12(2):230–236.
66. Li GB, et al. Mitochondrial fission and mitophagy depend on cofilin-mediated actin depolymerization activity at the mitochondrial fission site. *Oncogene*. 2018;37(11):1485–1502.
67. Fu Y, et al. Isoproterenol promotes rapid ryanodine receptor movement to bridging integrator 1 (BIN1)-organized dyads. *Circulation*. 2016;133(4):388–397.
68. Perry SW, Norman JP, Barbieri J, Brown EB, Gelbard HA. Mitochondrial membrane potential probes and the proton gradient: a practical usage guide. *BioTechniques*. 2011;50(2):98–115.
69. Readnower RD, Brainard RE, Hill BG, Jones SP. Standardized bioenergetic profiling of adult mouse cardiomyocytes. *Physiol Genomics*. 2012;44(24):1208–1213.
70. Hong T, et al. Cardiac BIN1 folds T-tubule membrane, controlling ion flux and limiting arrhythmia. *Nat Med*. 2014;20(6):624–632.
71. Smyth JW, et al. Limited forward trafficking of connexin 43 reduces cell cell coupling in stressed human and mouse myocardium. *J Clin Invest*. 2010;120(1):266–279.
72. Gao D, Zhang L, Dhillon R, Hong TT, Shaw RM, Zhu J. Dynasore protects mitochondria and improves cardiac lusitropy in Langendorff perfused mouse heart. *PLoS ONE*. 2013;8(4):e60967.
73. Kolk MV, et al. LAD-ligation: a murine model of myocardial infarction. *J Vis Exp*. 2009;(32):1438.
74. Redfors B, Shao Y, Omerovic E. Myocardial infarct size and area at risk assessment in mice. *Exp Clin Cardiol*. 2012;17(4):268–272.